Exaggerated inflammation, impaired host defense, and neuropathology in progranulin-deficient mice

Fangfang Yin,[1,4] Rebecca Banerjee,[2] Bobby Thomas,[2] Ping Zhou,[2,3] Liping Qian,[2,3] Ting Jia,[4] Xiaojing Ma,[1,4] Yao Ma,[1,5] Costantino Iadecola,[2,3] M. Flint Beal,[2] Carl Nathan,[1,4] and Aihao Ding[1,4]

[1]Department of Microbiology and Immunology, [2]Department of Neurology and Neuroscience, and [3]Division of Neurobiology, Weill Cornell Medical College, New York, NY 10065
[4]Graduate Program in Immunology and Microbial Pathogenesis, Weill Graduate School of Medical Sciences of Cornell University, New York, NY 10065
[5]Institute of Materia Medica, Chinese Academy of Medical Sciences, 100050 Beijing, China

Progranulin (PGRN) is a widely expressed protein involved in diverse biological processes. Haploinsufficiency of PGRN in the human causes tau-negative, ubiquitin-positive frontotemporal dementia (FTD). However, the mechanisms are unknown. To explore the role of PGRN in vivo, we generated PGRN-deficient mice. Macrophages from these mice released less interleukin-10 and more inflammatory cytokines than wild type (WT) when exposed to bacterial lipopolysaccharide. PGRN-deficient mice failed to clear *Listeria monocytogenes* infection as quickly as WT and allowed bacteria to proliferate in the brain, with correspondingly greater inflammation than in WT. PGRN-deficient macrophages and microglia were cytotoxic to hippocampal cells in vitro, and PGRN-deficient hippocampal slices were hypersusceptible to deprivation of oxygen and glucose. With age, brains of PGRN-deficient mice displayed greater activation of microglia and astrocytes than WT, and their hippocampal and thalamic neurons accumulated cytosolic phosphorylated transactivation response element DNA binding protein–43. Thus, PGRN is a key regulator of inflammation and plays critical roles in both host defense and neuronal integrity. FTD associated with PGRN insufficiency may result from many years of reduced neutrotrophic support together with cumulative damage in association with dysregulated inflammation.

CORRESPONDENCE
Aihao Ding:
ahding@med.cornell.edu

Abbreviations used: BAC, bacterial artificial chromosome; BMDM, bone marrow–derived macrophage; CAG, chicken actin gene; FTD, frontotemporal dementia; GFAP, glial fibrillary acidic protein; MCP-1, monocyte chemoattractant protein–1; OGD, oxygen and glucose deprivation; PGRN, progranulin; PI, propidium iodide; SLPI, secretory leukocyte protease inhibitor; TDP-43, transactivation response element DNA binding protein–43; TLR, Toll-like receptor.

Progranulin (PGRN), also known as proepithelin, acrogranin, or prostate cancer cell–derived growth factor (He and Bateman, 2003), is a secreted protein that undergoes proteolysis to generate seven mutually homologous 6-kD peptides, called GRNs or epithelins. Cysteine comprises 88 of PGRN's 593 residues and forms six intramolecular disulfide bridges in each of the GRNs, giving them a compact globular structure (Tolkatchev et al., 2008). PGRN is expressed by epithelial cells, macrophages, and neurons. Expression analyses and experiments with the native or recombinant protein have implicated PGRN in embryonic development, tumorigenesis, and wound healing (Daniel et al., 2000; Zhu et al., 2002; He and Bateman, 2003). A prominent role of PGRN in the regulation of inflammation was suggested by our discovery that neutrophil elastase and macrophage-derived secretory leukocyte protease inhibitor (SLPI) promote and prevent, respectively, the conversion of PGRN to GRNs, and that recombinant PGRN inhibits neutrophil activation, whereas GRNs promote epithelial cell generation of neutrophil chemoattractants (Zhu et al., 2002).

Mutations in the *PGRN* gene were recently found to cause frontotemporal dementia (FTD), the second most common dementia in people under the age of 65 (Neary et al., 1998). FTD patients experience gradual and progressive changes in behavior and personality, followed by a cognitive decline, prominent language disorders, and sometimes Parkinsonism, in association

The Rockefeller University Press $30.00
J. Exp. Med. Vol. 207 No. 1 117-128
www.jem.org/cgi/doi/10.1084/jem.20091568

The Journal of Experimental Medicine

with progressive cortical atrophy, neuronal loss, astrocytic gliosis, and microglial activation (Neary et al., 1998). At least 66 different pathogenic mutations in the *PGRN* gene have been documented in FTD patients, all of which resulted in functional null alleles and haploinsufficiency. These were associated with ubiqitinopathies, characterized by the deposit of ubiquitin-positive but tau-negative immunoreactivity in neuronal cytoplasmic and neuronal intranuclear inclusions (Mackenzie et al., 2006; Cairns et al., 2007; Josephs et al., 2007). One component of neuronal inclusions from PGRN-linked FTD patients was identified as transactivation response element DNA binding protein–43 (TDP-43; Neumann et al., 2006). Recent studies have linked pathological redistribution of TDP-43 from nuclei to cytoplasm to its phosphorylation and degradation (Cook et al., 2008; Hasegawa et al., 2008).

In this paper, we report that PGRN-deficient mice responded to infection with exaggerated inflammation. In vitro, their macrophages responded to microbial products by expressing enhanced levels of proinflammatory mediators and reduced antiinflammatory IL-10. Ex vivo, PGRN-deficient hippocampal neurons were more vulnerable than WT to metabolic stress. Finally, we detected microgliosis, astrocytosis, and cytoplasmic localization and phosphorylation of TDP-43 in the hippocampus and thalamus in aged PGRN-deficient mice but not in their WT counterparts. Thus, PGRN has a nonredundant role in modulating inflammatory responses. Our studies raise the possibility that FTD may result in part from brain damage arising from the combination of dysregulated inflammation and heightened neuronal vulnerability.

RESULTS

Generation of PGRN-deficient mice

Complete human PGRN deficiency has not been identified. Accordingly, we chose to make conditional PGRN knockout mice with the expectation that *pgrn* gene deletion might be embryonic lethal. We flanked the *pgrn* locus with *loxP* sites to bracket the promoter and the first four exons in a bacterial artificial chromosome (BAC) targeting vector (Fig. 1 A). Production of heterozygous and homozygous floxed mice was confirmed by Southern blotting (unpublished data). Generation of an all-tissue PGRN knockout was achieved by crossing *pgrn* floxed mice with mice transgenic for Cre recombinase driven by the promoter for the chicken actin gene (CAG; Fig. 1 B). This strategy left behind no neomycin resistance gene, as well as no Cre transgene, which can impart a phenotype (Schmidt-Supprian et al., 2007). Mature oocytes of CAG-Cre transgenic females contain sufficient Cre activity to mediate the deletion of paternally derived LoxP-flanked DNA sequences upon fertilization, irrespective of the transmission of the Cre transgene (Sakai and Miyazaki, 1997). In the mice used in this study, the PGRN-deficient mice and their WT littermates were Cre negative. PGRN mRNA levels in the knockout mice were undetectable in the intestine, spleen, skin, liver, kidney, and brain using a primer set that amplifies exons 7–10 (Fig. 1 C, left). Real-time RT-PCR likewise detected no messenger for PGRN using a primer set that amplifies exons 6 and 7 (Fig. 1 C, right). Immunostaining and Western blotting using polyclonal antibody against full-length PGRN confirmed that PGRN protein was markedly diminished in the brain (Fig. 1 D) and macrophages (Fig. 1 E) in PGRN-deficient mice. PGRN-deficient pups were born at the expected Mendelian frequency from hemizygous parents. Young-adult PGRN-deficient mice were healthy and fertile. Whole-body pathological evaluation was normal at the gross level, and there were no abnormalities in hematogram or serum chemistries (Table S1).

PGRN-deficient macrophages produce more proinflammatory cytokines and less antiinflammatory IL-10 than WT macrophages

PGRN binds to and is protected from degradation by another macrophage product, SLPI (Zhu et al., 2002). Like recombinant SLPI, recombinant PGRN has antiinflammatory effects (Jin et al., 1997; Zhu et al., 2002; Kessenbrock et al., 2008), but this function was only demonstrated by inhibition of neutrophil activation. To test the effect of depleting endogenous PGRN on inflammation, we stimulated bone marrow–derived macrophages (BMDMs) from PGRN-deficient mice with Toll-like receptor (TLR) agonists. Compared with WT BMDMs, PGRN-deficient BMDMs had similar cell-surface marker expression (Fig. S1) and phagocytic capacity (Fig. S2), but produced higher levels of transcripts and proteins for proinflammtory chemokines and cytokines such as monocyte chemoattractant protein–1 (MCP-1), CXCL1, IL-6, IL-12p40, and TNF (Fig. 2, A and B). In contrast, production of the antiinflammatory cytokine IL-10 was largely suppressed in PGRN-deficient BMDMs at the mRNA and protein levels (Fig. 2 C). The enhanced inflammatory responses illustrated for LPS (a TLR4 agonist) were recapitulated with Pam3CysSerLys4 (a ligand for TLR2), poly I:C (a ligand for TLR3), and hypomethylated bacterial DNA (a ligand for TLR9; Fig. S3). Thus, antiinflammatory effects of PGRN can be extended from restraining the cytokine response of neutrophils (Zhu et al., 2002) to regulating the cytokine production of macrophages.

PGRN synergizes with LPS in inducing IL-10 expression in macrophages

To test whether insufficient IL-10 induction from PGRN-deficient macrophages contributes to their overproduction of inflammatory cytokines, we stimulated BMDMs from WT and PGRN-deficient mice in the presence of a neutralizing antibody to IL-10 or control IgG. In the presence of anti–IL-10, WT macrophages produced as much TNF and MCP-1 as PGRN-deficient cells (Fig. 3 A), suggesting that compromised IL-10 production by PGRN-deficient macrophages does contribute to their hyperinflammatory phenotype. Next, we asked whether PGRN controls IL-10 expression at the transcriptional level. Nascent, unspliced IL-10 transcripts from WT and PGRN-deficient BMDMs after LPS stimulation were compared by quantitative real-time RT-PCR using a primer pair spanning the exon 2/intron 2 boundary

of the *il-10* gene. Fig. 3 B shows an ∼70% reduction of nascent IL-10 transcripts in PGRN-deficient cells. Thus, the defect in IL-10 expression in these cells is at least in part transcriptional. Finally, we tested the effect of recombinant PGRN (Zhu et al., 2002) on production of IL-10 from a mouse macrophage cell line, RAW264.7. Endotoxin-free PGRN alone did not induce IL-10 release by itself, but it synergized with LPS in a concentration-dependent fashion (Fig. 3 C).

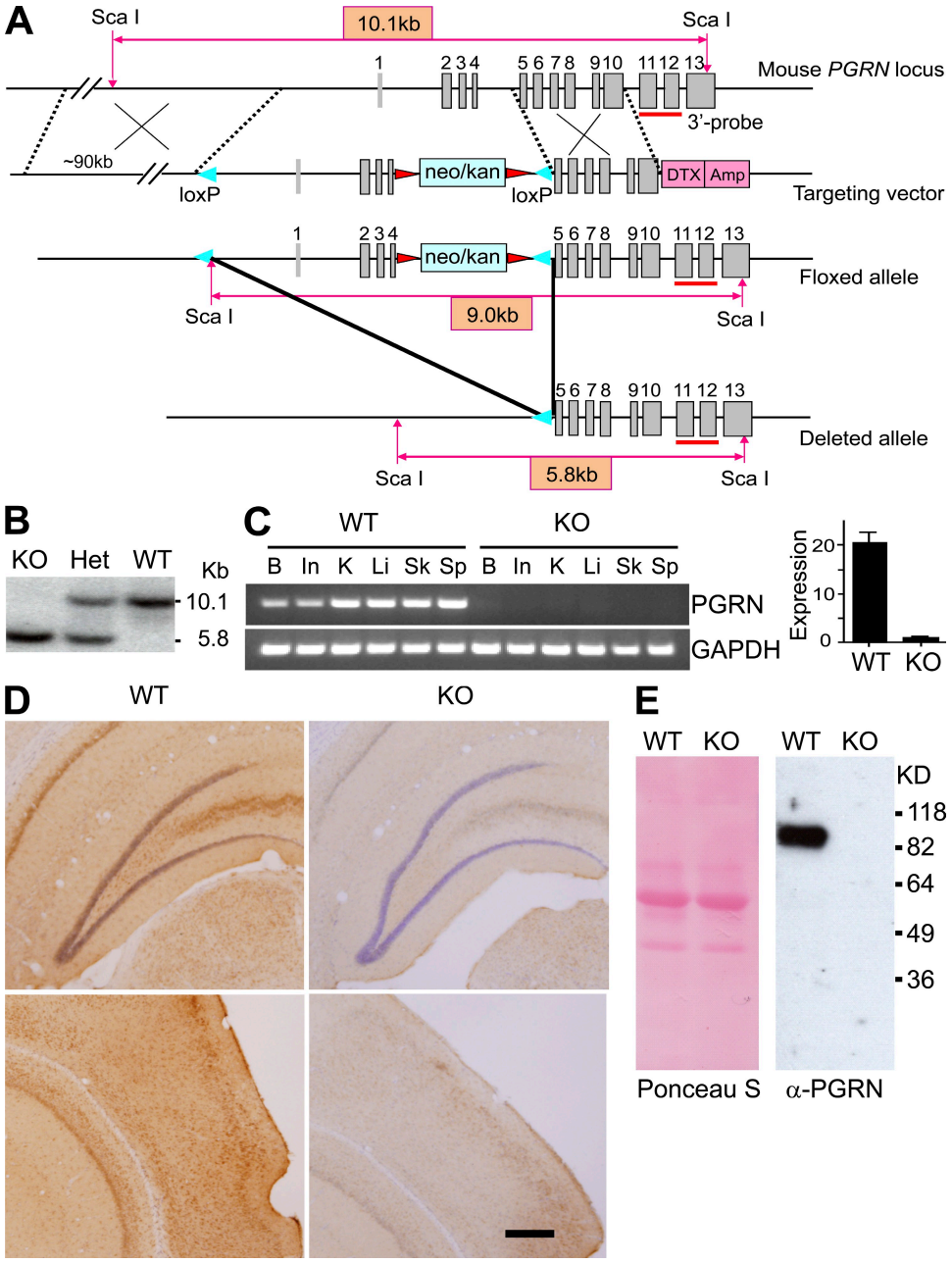

Figure 1. Generation of PGRN-deficient mice. (A) Mouse *pgrn* locus, targeting vector, and predicted floxed and deleted alleles. Gray boxes denote exons. Sequences are indicated for the neomycin/kanamycin resistance gene (neo/kan; light blue), diphtheria toxin/ampicillin gene (DTX/Amp; pink), LoxP sites (blue triangles), and flippase recombination target sites (red triangles). The red bar marks the 3′ probe. (B) Genotyping of PGRN-deficient mice after crossing PGRN floxed mice with CAG-Cre mice. Genomic DNA was restricted with *Sca*I for Southern blotting with the 3′ probe. Het, heterozygous; KO, homozygous knockout. (C) PGRN expression monitored by RT-PCR compared with GAPDH as a control (left). Quantification of PGRN transcripts in brain by real-time RT-PCR is shown (right). Results are means ± SEM. B, brain; In, intestine; K, kidney; Li, liver; Sk, skin; Sp, spleen. (D) Hippocampal (top) and cortical (bottom) sections from brains of WT and PGRN-deficient (KO) mice were stained with antibody against PGRN. Bar, 200 µm. (E) Mature BMDMs from 2-mo-old WT or PGRN-deficient mice (KO) were cultured in serum-free media for 48 h. Protein contents of conditioned media were blotted with anti-PGRN (right). Ponceau S staining of the same membrane is shown (left).

Thus, endogenous PGRN can serve as a negative regulator of inflammatory processes by helping to sustain the transcription of IL-10 during inflammation.

Bacterial infection of PGRN-deficient mice leads to exaggerated inflammatory tissue damage and delayed recovery

To test the role of endogenous PGRN during inflammation in vivo, we infected mice with *Listeria monocytogenes*, an intracellular pathogen widely used to study immune responses (Pamer, 2004; Serbina et al., 2008). PGRN-deficient mice had higher levels of MCP-1 in the serum, spleen, and brain than WT mice (Fig. 4 A). Paradoxically, high levels of MCP-1 in PGRN-deficient mice did not lead to more monocyte infiltration into infected organs. On the contrary, fewer monocytes were found in infected spleens of PGRN-deficient mice 24 h after infection (Fig. 4 B). This result is consistent with the report that overexpression of MCP-1 in transgenic mice disturbed the chemokine gradient and prevented timely monocyte infiltration into infected sites (Rutledge et al., 1995). As a consequence, PGRN-deficient mice had a high burden of *Listeria* in the spleen, liver, and brain at 5–7 d after infection, by which time few viable bacteria remained in WT mice (Fig. 4 C). Persistence of the infection was associated with a more sustained inflammatory response, as illustrated in the liver and brain (Fig. 4 D). Thus, PGRN-deficient mice may react to bacterial infections less efficiently than WT mice, resulting in excessive and prolonged inflammation.

Augmented age-dependent activation of microglia and astrocytes in the PGRN-deficient brain

To determine if there is any sign of dysregulated inflammation in the brains of PGRN-deficient mice, we examined the activation status of astrocytes and microglia, which help protect neurons from injury. Immunostaining of brain sections for myeloid antigen CD68, a marker for activated microglia, and glial fibrillary acidic protein (GFAP), an astrocytic marker, revealed little detectable difference between WT and PGRN-deficient mice at 3 mo of age (Fig. S4). Both CD68 and GFAP staining increased slightly with age. This increase was far more pronounced in the absence of PGRN (Fig. 5 A), particularly in the hippocampus, cortex, and thalamus (Fig. 5 A), where the increases in CD68- and GFAP-positive cells were statistically significant (Fig. 5 B). The age-dependent, reactive phenotype of microglia and astrocytes in the PGRN-deficient brain may be a primary consequence of PGRN deficiency in microglia and astrocytes, a compensatory response to damage in PGRN-deficient neurons, or both. The next sets of experiments explored these possibilities.

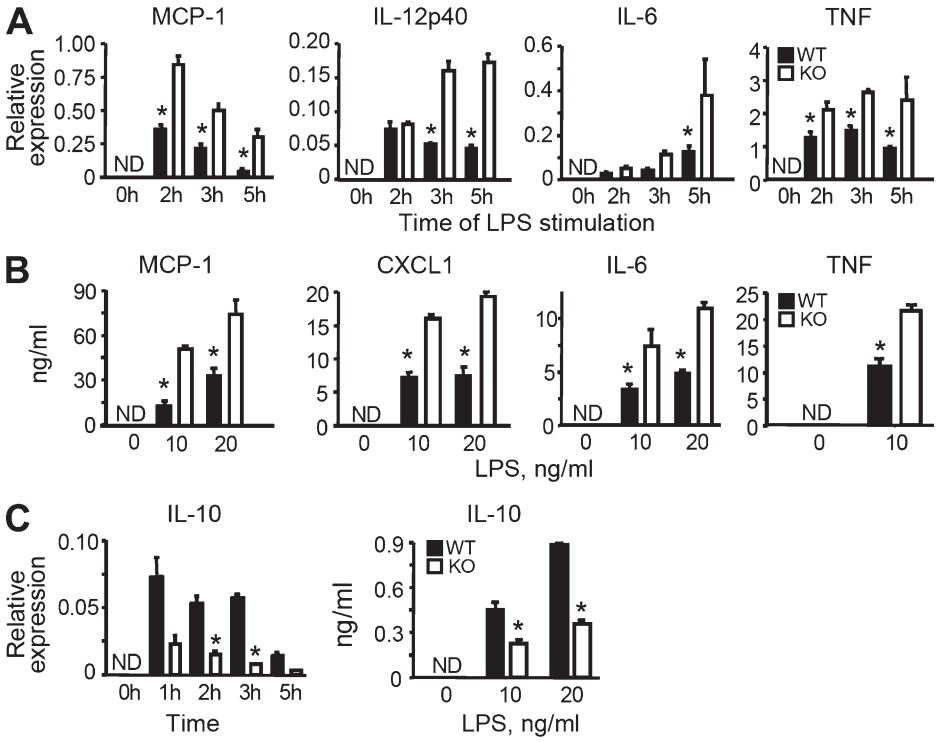

Figure 2. Dysregulated inflammatory responses of PGRN-deficient macrophages to bacterial endotoxin in vitro. (A) Reduced cytokine expression by PGRN-deficient macrophages in response to LPS. Quantitative RT-PCR at indicated times after exposure to 10 ng/ml LPS is shown. (B) Reduced cytokine release by PGRN-deficient macrophages in response to LPS. ELISAs were done with conditioned media collected 12 or 24 h after adding the indicated concentrations of LPS. (C) Enhanced IL-10 production by PGRN-deficient macrophages in response to LPS. IL-10 induction was determined as in A and B. Results are means ± SEM for triplicates from three to five similar experiments. *, $P < 0.05$ using the Student's *t* test. ND, nondetectable.

PGRN-deficient macrophages are more potent in killing hippocampal cells than WT macrophages

To test the potential impact of hyperinflammatory, PGRN-deficient myeloid cells on the brain, we incubated hippocampal slices from neonatal WT mice with BMDMs from PGRN-deficient mice or their WT littermates and measured brain cell death 5 d later by propidium iodide (PI) staining. LPS and IFN-γ were added to activate BMDMs. Unstimulated BMDMs caused minimal cell death. Stimulated WT BMDMs killed ∼18% of the cells in the hippocampal preparations, whereas PGRN-deficient BMDMs killed ∼50% (Fig. 6 A). This result suggests that the ability of activated macrophages to kill hippocampal cells is augmented in the absence of PGRN, consistent with the link of this deficiency to an exaggerated innate response phenotype (Fig. 2 and Fig. 4).

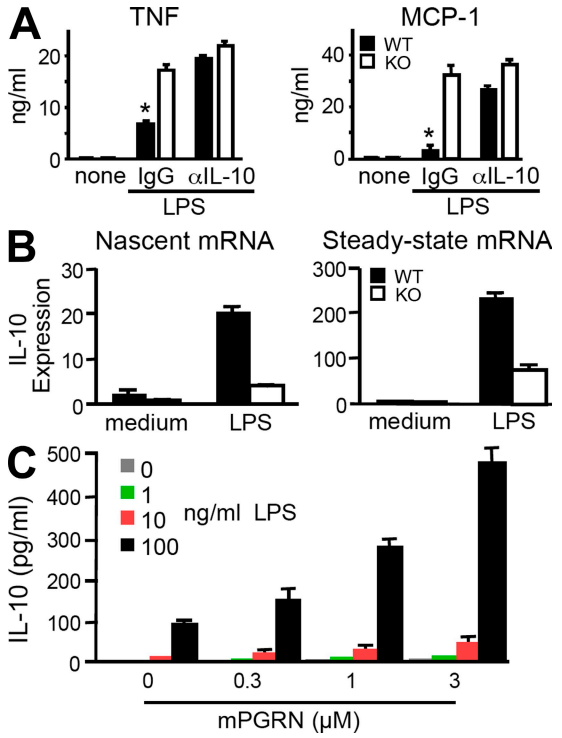

Figure 3. PGRN restrains macrophage inflammatory responses by synergizing with LPS for induction of IL-10 transcription. (A) Effect of anti–IL-10 antibody on TNF and MCP-1 production from BMDMs. 1 μg/ml anti–IL-10 or control IgG was added together with LPS and cytokines quantitated by ELISA as in Fig. 2 B. Results are expressed as means ± SEM of triplicate samples from one out of four experiments. (B) PGRN regulates IL-10 expression at the transcriptional level. Quantitative RT-PCR for nascent IL-10 transcripts (left) or spliced IL-10 transcripts (right) was measured 1 h after exposure of BMDMs to 100 ng/ml LPS. Results are expressed as means ± SEM of triplicate samples from one out of two independent experiments. (C) Recombinant PGRN synergized with LPS in IL-10 induction. RAW264.7 cells were incubated with the indicated concentrations of LPS and PGRN for 20 h. IL-10 in the conditioned media was measured by ELISA. Results are expressed as means ± SEM of three independent experiments. *, $P < 0.05$ using the Student's *t* test.

PGRN-deficient hippocampal slices are hypersusceptible to microglial activating agents and to deprivation of oxygen and glucose

To test whether PGRN-deficient microglia share this enhanced cell killing capacity, we expanded their numbers by treating hippocampal slices with GM-CSF for 3 d before adding LPS and IFN-γ (Duport and Garthwaite, 2005), and measured cell death 3 d later. Without GM-CSF pretreatment, minimum cell death was observed. After GM-CSF and LPS/IFN-γ treatment, cytotoxicity was more pronounced in PGRN-deficient hippocampal slices than in WT controls (Fig. 6 B). In the presence of neutralizing antibody against IL-10, WT microglia became as potent in killing hippocampal cells as PGRN-deficient microglia (Fig. 6 B). Thus, like macrophages, microglia cells control their inflammatory actions with balanced production of pro- and antiinflammatory mediators, among which IL-10 is a key modulator. Neutralizing endogenous IL-10 made WT microglia as neurotoxic as PGRN-deficient microglia.

To test the vulnerability of PGRN-deficient brain cells to a noninflammatory injury, we starved hippocampal slices for glucose and oxygen (Kawano et al., 2006; Kim et al., 2007). Cell death was greater in PGRN-deficient hippocampal tissues than in WT (Fig. 6 C). Thus, PGRN-deficient microglia respond to inflammatory stimuli by becoming more cytotoxic than WT microglia, and PGRN-deficient hippocampal tissues are more susceptible than WT to certain cytotoxic stresses, consistent with a neurotrophic role of this protein (Van Damme et al., 2008).

Increased ubiquitination and phosphorylation of TDP-43 in the PGRN-deficient brain

A neuropathological feature associated with PGRN-haploinsufficient FTD is the appearance of ubiquitin-positive neuronal cytoplasmic and intranuclear inclusions (Mackenzie et al., 2006), whose major component is TDP-43 (Neumann et al., 2006). We found that staining for ubiquitin was elevated in the hippocampus and thalamus but not other regions of 18-mo-old WT and PGRN-deficient mice, but was much more pronounced in PGRN-deficient mice (Fig. 7 A and Fig. S5). In our study, nuclear TDP-43 was detected in the hippocampus and thalamus at a similar level in WT and PGRN-deficient mice using a polyclonal antibody against full-length TDP-43 (Fig. 7 B, top). Whether TDP-43 colocalized with ubiquitin was difficult to confirm, because ubiquitination of autofluorescent lipofuscin was increased in the absence of PGRN (Lewis et al., 2009). However, the most striking change was the appearance of phospho–TDP-43 in the cytosol of neurons in the dentate gyrus and thalamus of aged PGRN-deficient but not aged WT mice (Fig. 7 B) or young PGRN-deficient mice (not depicted).

DISCUSSION

Contrary to expectations, PGRN proved to be dispensable during embryonic development of the mouse. This is consistent with the ability of another group to generate PGRN-deficient mice as well (Kayasuga et al., 2007). That study described

only one phenotype: altered male sexual behavior. The phenotypes observed in the present study reveal a profound role for endogenous PGRN in the balanced production of anti- and proinflammatory cytokines and chemokines. Although PGRN has been previously reported to be antiinflammatory (Zhu et al., 2002; Kessenbrock et al., 2008), this function was only shown with respect to inhibition of neutrophil activation, and the inference was based on the provision of exogenous, recombinant PGRN. The present work extends PGRN's antiinflammatory actions to inhibiting macrophage activation in vitro and global innate responses to bacterial infection in vivo, inferred in both cases from the effects of a loss of function mutation. Absence of PGRN led to overproduction of TNF and MCP-1 yet to a decreased ability to clear *Listeria*, with prolongation of inflammation in infected organs. In addition, we showed that PGRN exerted its antiinflammatory function in large part by synergizing with microbial products such as LPS to induce the transcription of IL-10, a major antiinflammatory cytokine. Further studies will address whether the immunodeficiency state we discovered in association with PGRN deficiency pertains to infectious agents other than *L. monocytogenes*.

Excessive proinflammatory responses have been implicated in many neurodegenerative diseases (González-Scarano and Baltuch, 1999; Minghetti, 2005; Lobsiger and Cleveland, 2007). In the brain, PGRN is widely expressed by different neuronal populations such as cortical and hippocampal pyramidal cells, as well as nonneuronal cells such as microglia. Trauma, malignancy, infection, and neurodegeneration are all associated with increased expression of PGRN in the brain (Liau et al., 2000; Ahmed et al., 2007; Pereson et al., 2009). The ability of PGRN to support resolution of inflammation

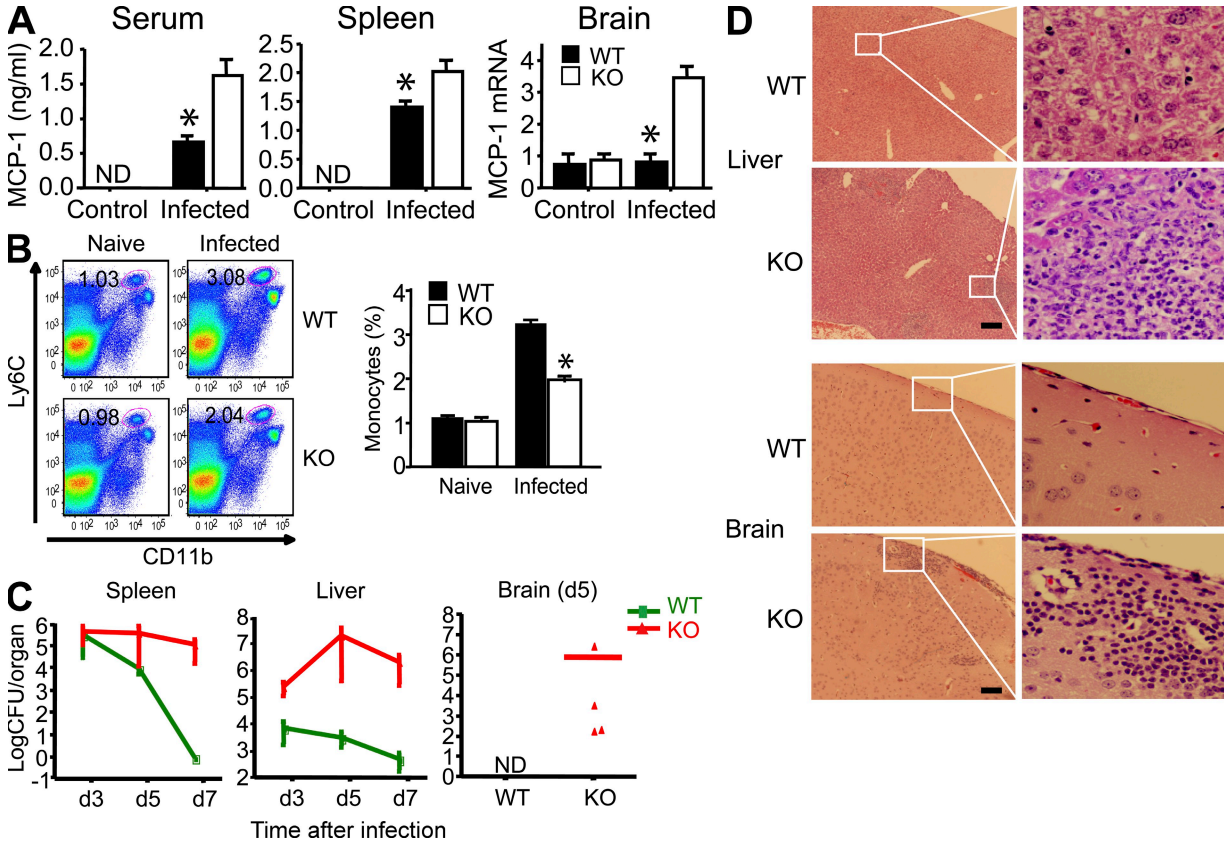

Figure 4. Defective host defense of PGRN-deficient mice. (A) Enhanced MCP-1 levels in PGRN-deficient mice in response to infection. WT and PGRN-deficient mice (n = 10 per group) were infected intravenously with 3×10^3 *L. monocytogenes*. MCP-1 levels in serum and spleen homogenates were determined 24 h after infection by ELISA. Hippocampal expression of MCP-1 was determined by real-time RT-PCR 5 d after infection and expressed as relative levels after normalization with GAPDH mRNA. Results are means ± SEM. *, $P < 0.05$ using the Student's t test. ND, nondetectable. (B) Decreased monocyte recruitment to infected spleens of PGRN-deficient mice. Cells from naive or infected spleen (24 h after infection) were tested for the expression of CD11b and Ly6C (for monocyte population). Numbers in dot plots indicate the percentage of $Ly6C^{hi}CD11b^{+}$ cells. Dot plots are of individual mice; bar graphs represent the mean of five mice per group. Experiments were repeated three times with similar results. *, $P < 0.05$ using the Student's t test. (C) Inability to rapidly resolve bacterial infection by PGRN-deficient mice. WT and PGRN-deficient (KO) mice were infected intravenously with 5×10^3 *L. monocytogenes*. Bacterial burdens in the spleen, liver, and brain were measured as CFUs at the times indicated (n = 5 per genotype for days 3 and 5 after infection; n = 10 per genotype for day 7 after infection). Results are means ± SEM from one out of three similar experiments. (D) Exaggerated tissue inflammation in PGRN-deficient mice, as assessed by hematoxylin and eosin staining at day 3 (liver) or 5 (brain) after intravenous infection with 5×10^3 *L. monocytogenes*. Results are means ± SEM from one out of three similar experiments. Bars, 200 µm.

suggests that increased PGRN in these settings may reflect a compensatory, antiinflammatory response. This is supported by two findings. First, we observed augmented, spontaneous, age-dependent activation of astrocytes and microglia in PGRN-deficient mice. Second, peripheral infection by *L. monocytogenes* resulted in much greater brain involvement in PGRN-deficient than in WT mice. This invites the speculation that a state of PGRN insufficiency in humans may be permissive for brain damage accumulating over decades from repeated episodes of inflammation.

Even under conditions of husbandry intended to avoid intercurrent infection, PGRN-deficient mice developed several neuropathological features as they aged for 18 mo, a short time in comparison to the age of human adults with FTD. For example, the widespread activation of microglia and astrocytes in aged PGRN-deficient mice was reminiscent of FTD. Moreover, cortical ubiquitin- and TDP-43–immunoreactive cytoplasmic or intranulear inclusions are common in FTD (Arai et al., 2006; Cairns et al., 2007; Josephs et al., 2007). We detected enhanced ubiquitination in the hippocampal and thalamic regions of aged PGRN-deficient mice. In addition, we detected cytosolic phosphorylated TPD-43 in the hippocampus and thalamus of aged PGRN-deficient mice and not in WT mice. However,

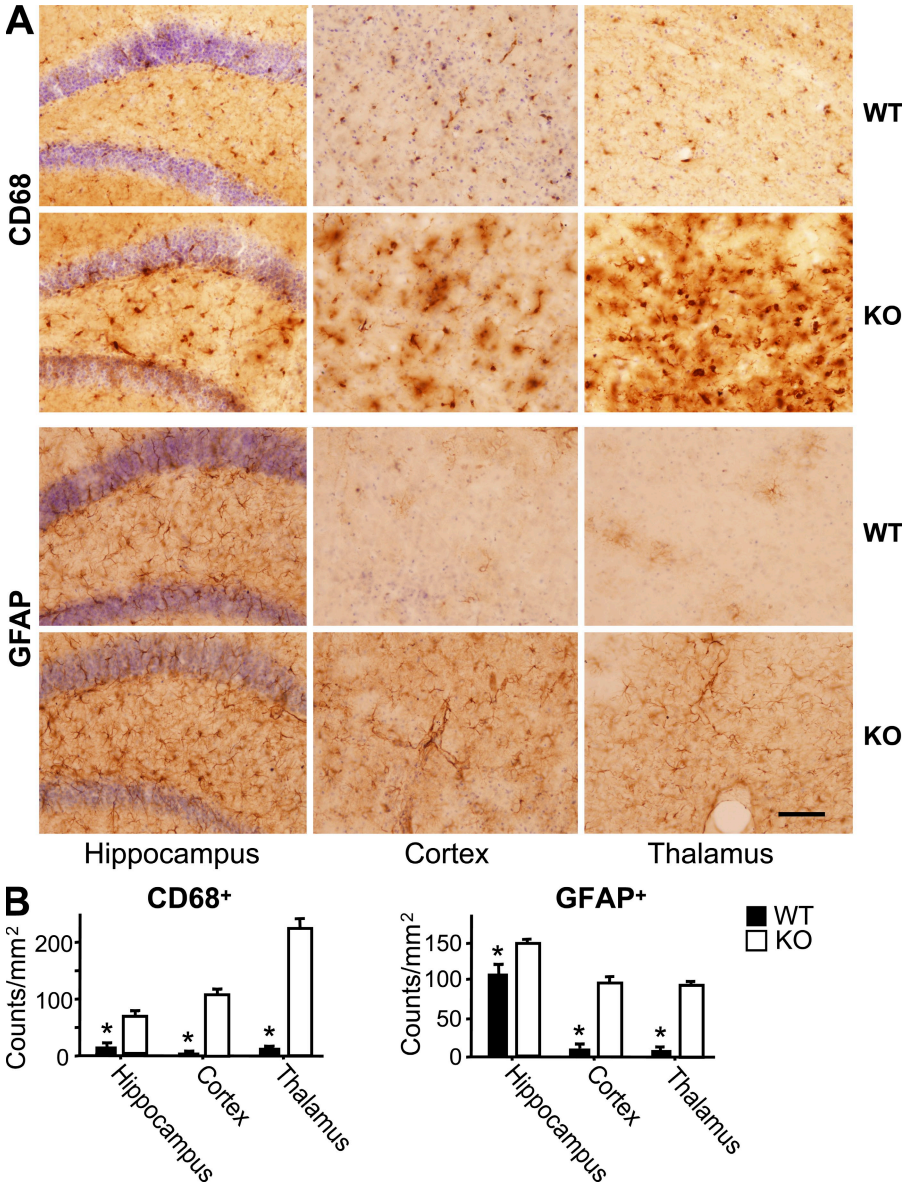

Figure 5. Augmented activation of microglia and astrocytes in the brain of aged PGRN-deficient mice. (A) Activation of microglia and astrocytes in PGRN-deficient mice. Hippocampal, cortical, and thalamic sections from 18-mo-old WT and PGRN-deficient (KO) mice ($n = 6$) were immunostained using antibody against CD68 or GFAP. (B) Activated CD68$^+$ and GFAP$^+$ cells were expressed as cells per square millimeter within indicated regions of both cerebral hemispheres of each animal. Results are means ± SEM from three independent experiments. *, $P < 0.01$ using the Student's *t* test. Bar, 80 µm.

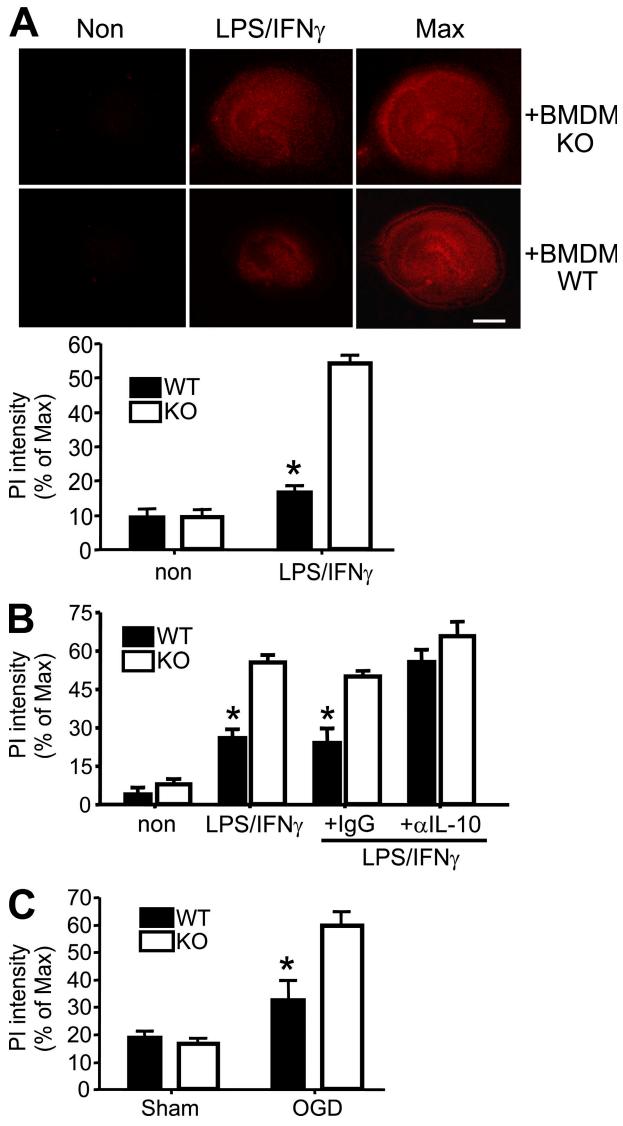

Figure 6. Enhanced neurotoxic potential of PGRN-deficient macrophages and microglia, and increased vulnerability of PGRN-deficient neurons to stress. (A) BMDM-induced cell death in cultured hippocampal slices. WT coronal hippocampal slices were incubated with WT ($n = 29$) or PGRN-deficient (KO; $n = 36$) BMDMs with (LPS/IFN-γ) or without (Non) LPS and IFN-γ for 5 d. Cell death was assessed with PI staining. (top) Representative images. (bottom) Quantitative evaluation is expressed as the percentage of PI staining relative to maximal PI staining (Max) induced with 0.1% Triton X-100. The results are means ± SEM from five independent experiments. *, $P < 0.001$ using the Student's *t* test. Bar, 1 mm. (B) Activated microglia-induced cell death in hippocampal slices. Slices ($n = 12$ per group) from WT or PGRN-deficient mice were incubated with 10 ng/ml GM-CSF (3 d), followed by stimulation with LPS and IFN-γ in the presence of 10 µg/ml anti–IL-10 or control IgG for 3 d. Cell death was measured as in A. The results are means ± SEM from three independent experiments. *, $P < 0.002$ using the Student's *t* test. (C) Effect of OGD on hippocampal slices from PGRN-deficient (KO) and WT mice ($n = 6$). Slices were cultured for 2 wk, followed by OGD treatment. Neuronal viability was assessed by PI staining before and after OGD. Maximal neuronal death was induced by exposure to 1 mM NMDA after OGD treatment. The results are means ± SEM from three independent experiments. *, $P < 0.001$ using the Student's *t* test.

in contrast to FTD, we did not detect neuropathology in the prefrontal or cortical regions of PGRN-deficient mice, and their distribution of phosphorylated TDP-43 differed from that of TDP-43 inclusions in human FTD. Most strikingly, our mice showed no evidence of cerebral atrophy within the period of study.

Aside from neuropathology, the mouse model in this study appears to differ from FTD in that no clinically apparent infectious or inflammatory phenotype has been reported in FTD patients to our knowledge, apart from increased MCP-1 and IL-8 levels in their cerebrospinal fluid (Galimberti et al., 2006). Perhaps the ∼50% deficiency of PGRN in FTD patients produces a less conspicuous defect than the near-total PGRN deficiency in this study. Conversely, it is formally possible, though unlikely, that hemizygosity for PGRN would result in a more extreme neuropathologic and less marked immunoinflammatory phenotype in mice than the homozygous PGRN deficiency in this study. Additionally or alternatively, a phenotype of prolonged infectious or inflammatory states in FTD patients in the decades preceding the onset of neuropsychiatric signs may have escaped attention. Our PGRN-deficient mice display specific behavioral abnormalities (unpublished data). It will be of interest to learn if those abnormalities progress as the mice age further, particularly under conditions in which they may experience repetitive bouts of infection or inflammation. Such conditions are routine in the wild but not in our mouse colony (Perry et al., 2007; Björkqvist et al., 2008). In sum, the reasons for the differences between the mice described in this paper and human FTD deserve further study. However, it is worth noting that no mouse model has yet recapitulated all the features of a human neurodegenerative disease.

It is unknown why haploinsufficiency in PGRN, a widely expressed protein, manifests chiefly by behavioral abnormalities and frontotemporal cerebral atrophy. A neurotrophic function of PGRN was first suggested by the ability of PGRN to promote the growth of PC12 cells, a pheochromocytoma-derived neuronal cell line (Daniel et al., 2000), and supported by the finding that granulin E improved survival and neurite growth of motor neurons in vitro (Van Damme et al., 2008). In this study, we demonstrated that PGRN-deficient macrophages, when activated, were more potent than WT macrophages in killing hippocampal neurons in co-culture. Moreover, neurons from PGRN-deficient mice were more vulnerable to damage by activated microglia and by the depletion of oxygen and glucose. Whether neurons from other regions of the brain share this vulnerability remains to be tested. Thus, FTD may arise from the congruence of two independent phenotypes of PGRN insufficiency: dysregulated inflammation and increased neuronal vulnerability to damage.

MATERIALS AND METHODS

Construction of a BAC targeting vector. A BAC clone containing the mouse WT *pgrn* locus was obtained from the Wellcome Trust Sanger Institute.

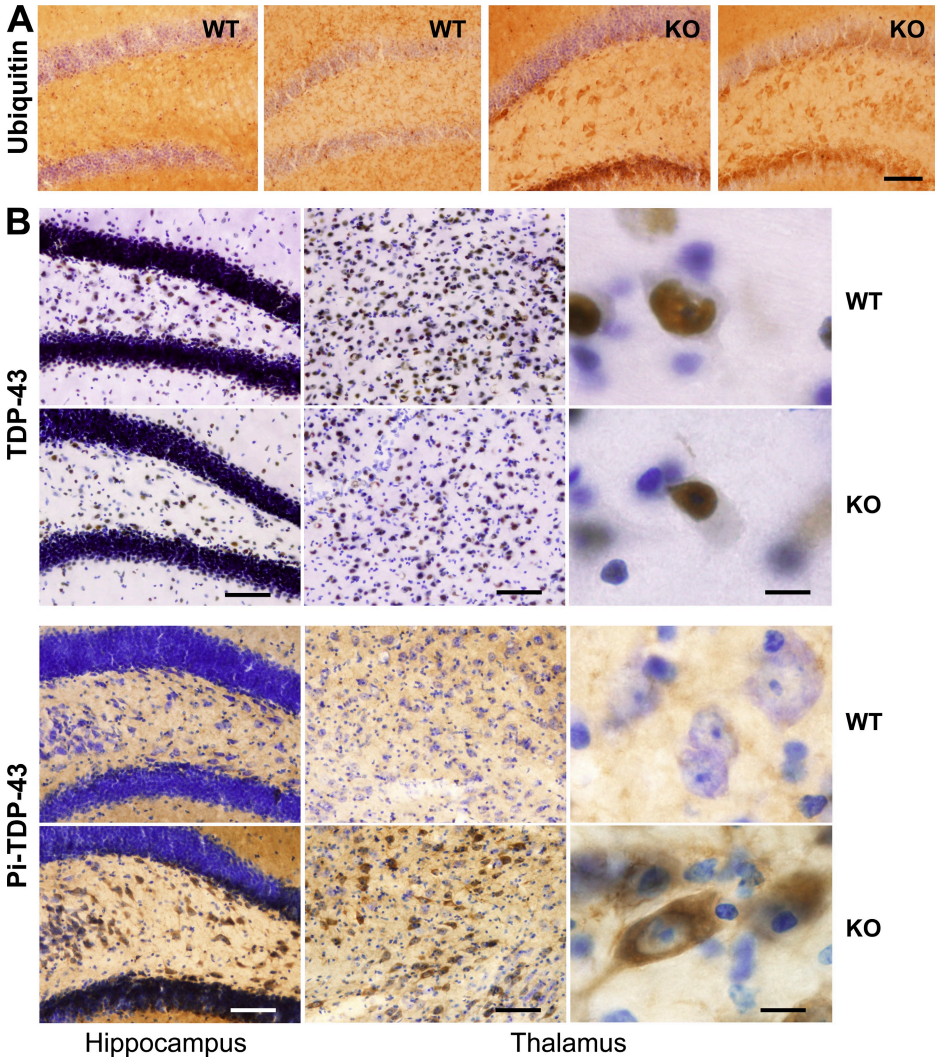

Figure 7. Increased ubiquitination and phosphorylation of TDP-43 in the PGRN-deficient brain. (A) Enhanced ubiquitin immunostaining in the hippocampus of old PGRN-deficient mice. Sections from 18-mo-old WT and PGRN-deficient (KO) mice ($n = 5$) were stained using antibody against ubiquitin. Representative sections from two different mice in each group are shown. Bar, 80 µm. (B) Phosphorylation of TDP-43 and its cytosolic translocation in aged PGRN-deficient (KO) mice. Hippocampal and thalamic sections from 18-mo-old WT and PGRN-deficient mice ($n = 5$) were stained with antibodies against TDP-43 (top) or phosphorylated TDP-43 (bottom). Bars: (left and middle) 80 µm; (right) 12 µm.

BAC recombineering machinery was provided by N. Copeland (National Cancer Institute, Bethesda, MD). The BAC modifications were made in a modified bacterial strain, SW102. This strain contains the λ prophage recombineering system and deficient galactokinase (*gal*K) gene. The three-step strategy for making this targeting vector is as follows. First, a PCR product containing a *lox*P site fused with a flippase recombination target–flanked neomycin/kanamycin (*neo/kan*) gene was introduced into the BAC clone and targeted into intron 4. The two 70 bp's of sequences homologous to the targeting site at both ends of this PCR product enabled precise targeting/homologous recombination. Kanamycin-resistant recombinants were selected. The second step was to insert a single *lox*P site into the 5′ end of the promoter region using galactose positive/negative selection. In brief, the *gal*K cassette, containing homology to the region 5′ of the *pgrn* promoter, was inserted into the BAC by homologous recombination. The recombinant bacteria grew on minimal media with galactose as the only carbon source (positive selection). Then the *gal*K cassette was substituted by an oligonucleotide with homology to the regions flanking the *gal*K cassette by selecting against bacteria with the *gal*K cassette by resistance to 2-deoxy-galactose (DOG) on minimal plates with glycerol as the only carbon source. This step is negative selection, as DOG phosphorylated by galactokinase is nonmetabolizable and therefore toxic. The last step was to insert a negative selection cassette for diphtheria toxin/ampicillin into the sequence after the last exon of the *pgrn* gene with the selection of both kanamycin- and ampicillin-resistant recombinants.

Generation of all-tissue PGRN knockout mice. 10 µg of the BAC targeting vector was linearized at a unique *PISce*-I site and electroporated into C2J embryonic stem (ES) cells with the C57BL/6 genetic background. 6 out of 96 ES cell clones selected with G418 and diphtheria toxin were identified as positive for homologous recombination by *Sca*I Southern blotting using 5′ and 3′ probes. Three positive ES clones were injected into C57BL/6 blastocysts by the Mouse Genetics Core Facility at Weill Cornell Medical College/Memorial Sloan-Kettering Cancer Center. Chimeras were identified and crossed with C57BL/6J to obtain the germline-transmitted heterozygous floxed mice ($pgrn^{flox/+}$) identified by *Sca*I Southern analysis. The heterozygous floxed mice are in a pure C57BL/6 background. Mating between two heterozygous mice generated homozygous floxed mice ($pgrn^{flox/flox}$).

CAG-Cre mice (four backcrosses to the C57BL/6 background from CD1 origin) were purchased from the Mouse Genetics Core Facility at Weill Cornell Medical College/Memorial Sloan-Kettering Cancer Center. Breeding of *pgrn*$^{flox/+}$ or *pgrn*$^{flox/flox}$ mice with CAG-Cre mice resulted in both Cre-positive and -negative mice with ubiquitous deletions of the *pgrn* gene and the *neo/kan* cassette. Experiments were performed using age- and sex-matched homozygous PGRN-deficient (Cre-negative) mice and their WT littermates. Animal studies were approved by the Institutional Animal Care and Use Committee of Weill Cornell Medical College.

Immunohistochemistry. Age- and sex-matched PGRN-deficient mice and their WT littermates were anesthetized with sodium pentobarbital and transcardially perfused with 0.9% saline followed by 4% paraformaldehyde (PFA) in PBS, pH 7.4. The brains were dissected out, postfixed in 4% PFA for 24 h, and cryopreserved in 30% sucrose/PBS for 48 h. Snap-frozen brains were embedded in tissue embedding freezing medium and sectioned at a 40-µm thickness using a cryostat. Coronal sections were collected in PBS and processed free floating for immunohistochemistry.

Coronal brain sections spanning the cortex, thalamus, and hippocampus were washed in PBS, and endogenous peroxidase was quenched by incubation in 3% hydrogen peroxide/10% methanol solution for 10 min. Sections were washed in PBS and blocked in 10% normal goat serum (NGS), 0.1% Triton X-100 in PBS for 1 h at room temperature. Next, sections were incubated with various antibodies: rabbit anti-PGRN (1:1,000; Zhu et al., 2002), rat monoclonal anti-CD68 (1:500; AbD Serotec), mouse monoclonal antiubiquitin (1:50,000; Millipore), rabbit polyclonal anti-GFAP (1:2,000; Dako), mouse monoclonal anti–phospho–TDP-43 (pS409/410; 1:500; provided by H. Akiyama, M. Hasegawa, and T. Arai, Tokyo Institute of Psychiatry, Tokyo, Japan; Inukai et al., 2008), and rabbit polyclonal anti–TDP-43 (Proteintech) in 2% NGS, 0.01% Triton X-100 in PBS for 16 h at 4°C. Sections were washed in PBS and incubated with appropriate biotinylated secondary antibodies (Jackson ImmunoResearch Laboratories, Inc.) in PBS for 1 h at room temperature. After incubation in streptavidin ABC enhancer solution (Vector Laboratories) for 30 min at room temperature, immunostaining was visualized with diaminobenzidine (DAB; Sigma-Aldrich) as the chromogen. Sections were washed and mounted on precoated slides (Superfrost Plus; VWR) and allowed to air dry. The sections were further counterstained with either cresyl violet acetate or thionin (Sigma-Aldrich). The slides were dehydrated in ascending series of ethanol, passed through xylene, and coverslipped with DPX mounting media (Electron Microscopy Science). Images were acquired using a digital camera (Coolpix 5000; Nikon).

Quantification of activated microglial cells and GFAP-reactive astrocytes. Microglial activation was quantitated by counts of CD68$^+$ cells exhibiting prominent amoeboid or activated morphology evident from DAB chromophore–stained sections, as previously described (Reynolds et al., 2007). GFAP-reactive astrocytes were counted in a similar fashion. Cell counts were compiled in an unbiased manner within the hippocampus, cortex, and thalamus by using Stereoinvestigator software (Microbrightfield) and expressed as cell numbers per square millimeter.

Western blotting for PGRN. Day 6 BMDMs were harvested and replated into a 6-well plate with two million cells/well in DMEM with 10% FBS. On the next day, the medium was changed into serum-free DMEM with or without additional stimulation. The conditioned medium was collected 48 h later, spun at 300 *g* for 5 min to remove cells, and precipitated with 20% trichloroacetic acid. The protein pellet was washed in 100% acetone and boiled immediately in 2× SDS Laemmli loading dye. The antibody anti-PGRN was as previously described (Zhu et al., 2002).

Culture of BMDMs. Bone marrow cells flushed from mouse femurs (day 0) were cultured in DMEM supplemented with 20% L929 conditioned medium and 20% heat-inactivated FBS for 6 d, with fresh medium replenished on day 4. Day 6 BMDMs were harvested in ice-cold PBS and replated according to different experimental purposes.

Phagocytosis assay. This assay was performed according to the manufacturer's protocol (Invitrogen). BMDMs were plated into 96-well black plates at 10^5 cells/well (BD) in 100 µl of complete DMEM and incubated at 37°C for 2 h. After the culture medium was removed, 100 µl of sonicated fluorescent-labeled *Escherichia coli* was added to all wells for another 2 h. The *E. coli* suspension was then removed, and 100 µl of Trypan blue was added for 1 min at room temperature and then aspirated. We measured fluorescence at 480 nm excitation/520 nm emission and calculated relative fluorescence by subtracting the fluorescence of control wells containing macrophages but without *E. coli* and the fluorescence from wells containing *E. coli* but without macrophages. Each group included four wells.

RT-PCR and quantitative real-time RT-PCR. PGRN expression in different organs was determined via RT-PCR using RNA from organs of 2-mo-old WT and PGRN-deficient mice as templates, and amplified with a primer set that covers exons 7–10 (forward primer, 5′-CTGTCGTGTGCCCTGATGCTAAG-3′; reverse primer, 5′-CCCCAGTCCCCAGAATTGAGTTTG-3′). To quantify PGRN expression in the brain, the brain was lysed in TRIzol (Invitrogen) and total RNA was extracted with the RNeasy Mini Kit (QIAGEN). 100 ng RNA was transcribed into cDNA with a random hexamer. Real-time RT-PCR was performed on a sequence detection system (ABI PRISM 7900HT; Applied Biosystems) using a primer set that covers exons 6 and 7 (forward primer, 5′-GTTCCCTGCACAAAAGACCAA-3′; reverse primer, 5′-GGGTCTTAGCATCAGGGCAC-3′; Taqman probe, 5′-AGGGCAGTGTCTTTGCCTTTTTCTGTCG-3′). To determine cytokine expression in macrophages, cells were stimulated with LPS. At various times after stimulation, total RNA was extracted and reverse transcribed, and real-time PCR was performed as described. The primer sequences for cytokines in real-time RT-PCR are as follows: TNF-α (forward primer, 5′-TGCTTGTTGACAGCGGTCC-3′; reverse primer, 5′-ACTGGCCATCGTGGAGGTAC-3′; probe, 5′-AGGGCAGTGTGTTACGTGCAGTGACAA-3′), MCP-1 (forward primer, 5′-GAGCATCCACGTGTTGGCT-3′; reverse primer, 5′-TGGTGAATGAGTAGCAGCAGGT-3′; probe, 5′-AGCCAGATGCAGTTAACGCCCCACT-3′), IL-12P40 (forward primer, 5′-GAGCAGTAGCAGTTCCCTGA-3′; reverse primer, 5′-TCCAGTGTGACCTTCTCTGCA-3′; probe, 5′-TCTCGGGCAGTGACATGTGGAATGG-3′), IL-6 (forward primer, 5′-CCCAATTTCCAATGCTCTCC-3′; reverse primer, 5′-TGAATTGGATGGTCTTGGTCC-3′; probe, 5′-AACAGATAAGCTGGAGTCACAGAAGGAGTGGC-3′), GAPDH (forward primer, 5′-GGGAAGCCCATCACCATCTT-3′; reverse primer, 5′-ACATACTCAGCACCGGCCTC-3′; probe, 5′-AGCGAGACCCCACTAACATCAAATGGG-3′), and IL-10 (forward primer, 5′-AGACCCTCAGGATGCGGC-3′; reverse primer, 5′-CCACTGCCTTGCTCTTATTTTCA-3′; probe, 5′-AGGCGCTGTCATCGATTTCTCCCCT-3′). For nascent IL-10 transcript determination, we used a primer set spanning the boundary of exon 2/intron 2 (forward primer, 5′-AAGGACCAGCTGGACAACAT-3′; reverse primer, 5′-TTCACAACCCTTGACTGCTG-3′). The amount of mRNA was expressed as copies of mRNA/copy of GAPDH mRNA.

ELISA. Day 6 BMDMs were harvested and replated into a 96-well plate at 100,000 cells/well. 2 h after plating, the cells were stimulated with LPS. At 12, 24, or 48 h after stimulation, the medium was collected and measured for cytokine levels with ELISA kits from R&D Systems according to the manufacturer's protocol.

Hippocampal slice culture and BMDM-induced hippocampal cell death. Hippocampi were dissected aseptically from 6-d-old male WT and PGRN-deficient pups. 350-µm coronal slices were obtained using a McIlwain Tissue Chopper (Vibratome Company). The slices were placed onto a Millicell culture insert and cultured for 13 d in medium containing 25% horse serum, 50% Eagles' basal medium, 25% HBSS, and 5 mg/ml glucose. Medium was changed twice a week. To induce cell death in slices with activated BMDMs, slices were incubated with 10^5 BMDMs for 5 d in the absence or presence of 5 µg/ml LPS and 100 U/ml IFN-γ. Cell death in hippocampal

slices was assessed by staining with 5 μg/ml PI. Fluorescence images were taken to assess the percentage of cell death using a fluorescence microscope (Eclipse; Nikon) equipped with a digital camera (Retiga Exi; QImaging) connected to a computer (Macintosh) running IPLab software (Scanalytics, Inc.). Maximal cell death was achieved by exposing the same hippocampal slice to 0.1% Triton X-100. The percentage of cell death in each slice was calculated based on the PI fluorescence intensity in images taken before and after treatment, and expressed as the percentage of maximal cell death, as previously described (Kim et al., 2007).

Microglia-induced hippocampal cell death. Microglia in hippocampal slices were expanded by incubation with 10 ng/ml G-CSF for 3 D, which has been shown to increase microglial populations by 50% (Duport and Garthwaite, 2005). The microglial cell population was activated with 1 μg/ml LPS and 100 U/ml IFN-γ for 3 d. Cell death was assessed as described.

Oxygen and glucose deprivation (OGD). Hippocampal slices from PGRN-deficient mice and their WT littermates were cultured for 13 d before being treated for OGD. The procedures for OGD and assessment of neuronal injury were as previously described (Kim et al., 2007). In brief, slices were first washed with OGD buffer (125 mM NaCl, 5 mM KCl, 1.2 mM NaH_2PO_4, 26 mM $NaHCO_3$, 1.8 mM $CaCl_2$, 0.9 mM $MgCl_2$, 10 mM Hepes, pH 7.2), followed by incubation in nitrogen-flushed OGD buffer in a sealed chamber filled with 95% N_2 and 5% CO_2 for 45 min at 37°C. The slices were then returned to normal culture medium and incubated in normal culture conditions for an additional 24 h. Cell death was assessed by PI staining and calculated as described.

***L. monocytogenes* infection.** Sex- and age-matched mice were infected intravenously with 5,000 *L. monocytogenes* strain 10403S. At various times after infection, serum, spleens, livers, and brains were collected. Bacterial CFUs were determined by plating serial dilutions of the homogenates on brain–heart infusion agar and incubating the plates at 37°C overnight. For tissue pathology, livers and brains from WT and PGRN-deficient mice were dissected on day 3 or 5 after infection, and fixed in 10% neutral formalin buffer overnight at room temperature. Sections (~10 μm thick) were prepared from microtome and stained with hematoxylin and eosin. For in vivo cytokine production and monocyte recruitment experiments, mice were infected intravenously with 3,000 *L. monocytogenes* and analyzed 24 h after infection.

Flow cytometry analysis. Splenocytes were subjected to flow cytometry using the following antibodies purchased from BD: anti-CD11b–PerCP (M1/70), anti-CD11c–allophycocyanin (APC), anti-Ly6C–FITC (AL-21), anti-Ly6G–PE, anti-CD4–FITC, anti-CD16/32–PE, anti-CD18–APC, and anti-F4/80–PE. For flow cytometry analysis, a large forward scatter/side scatter gate was drawn to include lymphocyte/monocyte populations. The samples were analyzed with flow cytometers (FACSCalibur or LSR; BD).

Statistical analyses. Statistical analyses were performed using the two-tailed Student's *t* test for independent samples. $P < 0.05$ was considered statistically significant. All data are presented as means ± SEM.

Online supplemental material. Table S1 shows that young PGRN-deficient mice have no morphological, hematologic, or biochemical abnormalities. Figs. S1 and S2 indicate that macrophages from WT and PGRN-deficient mice have similar surface markers and phagocytic capacity. Fig. S3 shows that PGRN-deficient macrophages displayed exaggerated inflammatory responses to other TLR ligands. Fig. S4 shows CD68 and GFAP staining of the hippocampus, cortex, and thalamus of 3- or 18-mo-old WT and PGRN-deficient mice. Fig. S5 shows ubiquitin staining of the hippocampus and thalamus of 3- or 18-mo-old WT and PGRN-deficient mice. Online supplemental material is available at http://www.jem.org/cgi/content/full/jem.20091568/DC1.

We thank H. Li, N. Chan, and R. McDonald for technical help; E. Pamer for helpful discussion; N. Copeland for reagents and protocols for BAC recombineering; and H. Akiyama, M. Hasegawa, and T. Arai for the antibody against phosphorylated TDP-43.

This work was supported by National Institutes of Health grants GM061710 (to A. Ding), NS060885 (to B. Thomas), and NS34179 and NS35806 (to C. Iadecola); a predoctoral fellowship from the Cancer Research Institute (to F. Yin); and an Appel Established Investigatorship (to C. Nathan). The Department of Microbiology and Immunology is supported by the William Randolph Hearst Foundation.

The authors declare no competing financial interests.

Submitted: 20 July 2009
Accepted: 17 November 2009

REFERENCES

Ahmed, Z., I.R. Mackenzie, M.L. Hutton, and D.W. Dickson. 2007. Progranulin in frontotemporal lobar degeneration and neuroinflammation. *J. Neuroinflammation.* 4:7. doi:10.1186/1742-2094-4-7

Arai, T., M. Hasegawa, H. Akiyama, K. Ikeda, T. Nonaka, H. Mori, D. Mann, K. Tsuchiya, M. Yoshida, Y. Hashizume, and T. Oda. 2006. TDP-43 is a component of ubiquitin-positive tau-negative inclusions in frontotemporal lobar degeneration and amyotrophic lateral sclerosis. *Biochem. Biophys. Res. Commun.* 351:602–611. doi:10.1016/j.bbrc.2006.10.093

Björkqvist, M., E.J. Wild, J. Thiele, A. Silvestroni, R. Andre, N. Lahiri, E. Raibon, R.V. Lee, C.L. Benn, D. Soulet, et al. 2008. A novel pathogenic pathway of immune activation detectable before clinical onset in Huntington's disease. *J. Exp. Med.* 205:1869–1877. doi:10.1084/jem.20080178

Cairns, N.J., M. Neumann, E.H. Bigio, I.E. Holm, D. Troost, K.J. Hatanpaa, C. Foong, C.L. White III, J.A. Schneider, H.A. Kretzschmar, et al. 2007. TDP-43 in familial and sporadic frontotemporal lobar degeneration with ubiquitin inclusions. *Am. J. Pathol.* 171:227–240. doi:10.2353/ajpath.2007.070182

Cook, C., Y.J. Zhang, Y.F. Xu, D.W. Dickson, and L. Petrucelli. 2008. TDP-43 in neurodegenerative disorders. *Expert Opin. Biol. Ther.* 8:969–978. doi:10.1517/14712598.8.7.969

Daniel, R., Z. He, K.P. Carmichael, J. Halper, and A. Bateman. 2000. Cellular localization of gene expression for progranulin. *J. Histochem. Cytochem.* 48:999–1009.

Duport, S., and J. Garthwaite. 2005. Pathological consequences of inducible nitric oxide synthase expression in hippocampal slice cultures. *Neuroscience.* 135:1155–1166. doi:10.1016/j.neuroscience.2005.06.035

Galimberti, D., N. Schoonenboom, P. Scheltens, C. Fenoglio, E. Venturelli, Y.A. Pijnenburg, N. Bresolin, and E. Scarpini. 2006. Intrathecal chemokine levels in Alzheimer disease and frontotemporal lobar degeneration. *Neurology.* 66:146–147. doi:10.1212/01.wnl.0000191324.08289.9d

González-Scarano, F., and G. Baltuch. 1999. Microglia as mediators of inflammatory and degenerative diseases. *Annu. Rev. Neurosci.* 22:219–240.

Hasegawa, M., T. Arai, T. Nonaka, F. Kametani, M. Yoshida, Y. Hashizume, T.G. Beach, E. Buratti, F. Baralle, M. Morita, et al. 2008. Phosphorylated TDP-43 in frontotemporal lobar degeneration and amyotrophic lateral sclerosis. *Ann. Neurol.* 64:60–70. doi:10.1002/ana.21425

He, Z., and A. Bateman. 2003. Progranulin (granulin-epithelin precursor, PC-cell-derived growth factor, acrogranin) mediates tissue repair and tumorigenesis. *J. Mol. Med.* 81:600–612. doi:10.1007/s00109-003-0474-3

Inukai, Y., T. Nonaka, T. Arai, M. Yoshida, Y. Hashizume, T.G. Beach, E. Buratti, F.E. Baralle, H. Akiyama, S. Hisanaga, and M. Hasegawa. 2008. Abnormal phosphorylation of Ser409/410 of TDP-43 in FTLD-U and ALS. *FEBS Lett.* 582:2899–2904. doi:10.1016/j.febslet.2008.07.027

Jin, F.Y., C. Nathan, D. Radzioch, and A. Ding. 1997. Secretory leukocyte protease inhibitor: a macrophage product induced by and antagonistic to bacterial lipopolysaccharide. *Cell.* 88:417–426. doi:10.1016/S0092-8674(00)81880-2

Josephs, K.A., Z. Ahmed, O. Katsuse, J.F. Parisi, B.F. Boeve, D.S. Knopman, R.C. Petersen, P. Davies, R. Duara, N.R. Graff-Radford, et al. 2007. Neuropathologic features of frontotemporal lobar degeneration with ubiquitin-positive inclusions with progranulin gene (PGRN) mutations. *J. Neuropathol. Exp. Neurol.* 66:142–151. doi:10.1097/nen.0b013e31803020cf

Kawano, T., J. Anrather, P. Zhou, L. Park, G. Wang, K.A. Frys, A. Kunz, S. Cho, M. Orio, and C. Iadecola. 2006. Prostaglandin E2 EP1 receptors:

downstream effectors of COX-2 neurotoxicity. *Nat. Med.* 12:225–229. doi:10.1038/nm1362

Kayasuga, Y., S. Chiba, M. Suzuki, T. Kikusui, T. Matsuwaki, K. Yamanouchi, H. Kotaki, R. Horai, Y. Iwakura, and M. Nishihara. 2007. Alteration of behavioural phenotype in mice by targeted disruption of the progranulin gene. *Behav. Brain Res.* 185:110–118. doi:10.1016/j.bbr.2007.07.020

Kessenbrock, K., L. Fröhlich, M. Sixt, T. Lämmermann, H. Pfister, A. Bateman, A. Belaaouaj, J. Ring, M. Ollert, R. Fässler, and D.E. Jenne. 2008. Proteinase 3 and neutrophil elastase enhance inflammation in mice by inactivating antiinflammatory progranulin. *J. Clin. Invest.* 118:2438–2447.

Kim, Y., P. Zhou, L. Qian, J.Z. Chuang, J. Lee, C. Li, C. Iadecola, C. Nathan, and A. Ding. 2007. MyD88-5 links mitochondria, microtubules, and JNK3 in neurons and regulates neuronal survival. *J. Exp. Med.* 204:2063–2074. doi:10.1084/jem.20070868

Lewis, J.M., Z. Ahmed, H. Sheng, Y.-F. Xu, W.-L. Lin, A. Innes, H. Hou, M.L. Huttom, E. McGawan, and D.W. Dickson. 2009. Neuropathological characterization of progranulin-deficient mice: accelerated lipofuscin accumulation suggests a role for progranulin in successful aging. *Alzheimers Dement.* 5(Suppl.):P161–P162.

Liau, L.M., R.L. Lallone, R.S. Seitz, A. Buznikov, J.P. Gregg, H.I. Kornblum, S.F. Nelson, and J.M. Bronstein. 2000. Identification of a human glioma-associated growth factor gene, granulin, using differential immuno-absorption. *Cancer Res.* 60:1353–1360.

Lobsiger, C.S., and D.W. Cleveland. 2007. Glial cells as intrinsic components of non-cell-autonomous neurodegenerative disease. *Nat. Neurosci.* 10:1355–1360. doi:10.1038/nn1988

Mackenzie, I.R., M. Baker, S. Pickering-Brown, G.Y. Hsiung, C. Lindholm, E. Dwosh, J. Gass, A. Cannon, R. Rademakers, M. Hutton, and H.H. Feldman. 2006. The neuropathology of frontotemporal lobar degeneration caused by mutations in the progranulin gene. *Brain.* 129:3081–3090. doi:10.1093/brain/awl271

Minghetti, L. 2005. Role of inflammation in neurodegenerative diseases. *Curr. Opin. Neurol.* 18:315–321. doi:10.1097/01.wco.0000169752.54191.97

Neary, D., J.S. Snowden, L. Gustafson, U. Passant, D. Stuss, S. Black, M. Freedman, A. Kertesz, P.H. Robert, M. Albert, et al. 1998. Frontotemporal lobar degeneration: a consensus on clinical diagnostic criteria. *Neurology.* 51:1546–1554.

Neumann, M., D.M. Sampathu, L.K. Kwong, A.C. Truax, M.C. Micsenyi, T.T. Chou, J. Bruce, T. Schuck, M. Grossman, C.M. Clark, et al. 2006. Ubiquitinated TDP-43 in frontotemporal lobar degeneration and amyotrophic lateral sclerosis. *Science.* 314:130–133. doi:10.1126/science.1134108

Pamer, E.G. 2004. Immune responses to *Listeria monocytogenes*. *Nat. Rev. Immunol.* 4:812–823. doi:10.1038/nri1461

Pereson, S., H. Wils, G. Kleinberger, E. McGowan, M. Vandewoestyne, B. Van Broeck, G. Joris, I. Cuijt, D. Deforce, M. Hutton, et al. 2009. Progranulin expression correlates with dense-core amyloid plaque burden in Alzheimer disease mouse models. *J. Pathol.* 219:173–181. doi:10.1002/path.2580

Perry, V.H., C. Cunningham, and C. Holmes. 2007. Systemic infections and inflammation affect chronic neurodegeneration. *Nat. Rev. Immunol.* 7:161–167. doi:10.1038/nri2015

Reynolds, A.D., R. Banerjee, J. Liu, H.E. Gendelman, and R.L. Mosley. 2007. Neuroprotective activities of CD4+CD25+ regulatory T cells in an animal model of Parkinson's disease. *J. Leukoc. Biol.* 82:1083–1094. doi:10.1189/jlb.0507296

Rutledge, B.J., H. Rayburn, R. Rosenberg, R.J. North, R.P. Gladue, C.L. Corless, and B.J. Rollins. 1995. High level monocyte chemoattractant protein-1 expression in transgenic mice increases their susceptibility to intracellular pathogens. *J. Immunol.* 155:4838–4843.

Sakai, K., and J. Miyazaki. 1997. A transgenic mouse line that retains Cre recombinase activity in mature oocytes irrespective of the cre transgene transmission. *Biochem. Biophys. Res. Commun.* 237:318–324. doi:10.1006/bbrc.1997.7111

Schmidt-Supprian, M., F.T. Wunderlich, and K. Rajewsky. 2007. Excision of the Frt-flanked neo (R) cassette from the CD19cre knock-in transgene reduces Cre-mediated recombination. *Transgenic Res.* 16:657–660. doi:10.1007/s11248-007-9100-4

Serbina, N.V., T. Jia, T.M. Hohl, and E.G. Pamer. 2008. Monocyte-mediated defense against microbial pathogens. *Annu. Rev. Immunol.* 26:421–452. doi:10.1146/annurev.immunol.26.021607.090326

Tolkatchev, D., S. Malik, A. Vinogradova, P. Wang, Z. Chen, P. Xu, H.P. Bennett, A. Bateman, and F. Ni. 2008. Structure dissection of human progranulin identifies well-folded granulin/epithelin modules with unique functional activities. *Protein Sci.* 17:711–724. doi:10.1110/ps.073295308

Van Damme, P., A. Van Hoecke, D. Lambrechts, P. Vanacker, E. Bogaert, J. van Swieten, P. Carmeliet, L. Van Den Bosch, and W. Robberecht. 2008. Progranulin functions as a neurotrophic factor to regulate neurite outgrowth and enhance neuronal survival. *J. Cell Biol.* 181:37–41. doi:10.1083/jcb.200712039

Zhu, J., C. Nathan, W. Jin, D. Sim, G.S. Ashcroft, S.M. Wahl, L. Lacomis, H. Erdjument-Bromage, P. Tempst, C.D. Wright, and A. Ding. 2002. Conversion of proepithelin to epithelins: roles of SLPI and elastase in host defense and wound repair. *Cell.* 111:867–878. doi:10.1016/S0092-8674(02)01141-8